

PACS numbers: 42.55.Px; 42.60.Jf; 42.60.Da
DOI: 10.1070/QE2005v035n06ABEH006617

Quality of the optical beam of a high-power, single-mode, 0.81-μm ridge AlGaAs heterolaser

S.A. Plisyuk, I.V. Akimova, A.E. Drakin, A.V. Borodaenko,
A.A. Stratonnikov, V.V. Popovichev, A.P. Bogatov

***Abstract*. The parameters of a 0.81-μm ridge heterolaser are optimised by using the procedure developed earlier. As a result, 200 mW of the single-mode output is obtained in a diffraction-limited beam. It is shown experimentally that the near-field two-dimensional intensity distribution of the lasers under study can be well represented in the factorised form, which demonstrates the applicability of the 'effective' refractive index method for simulating these lasers.**

Keywords: *heterolaser, diffraction-limited divergence, brightness.*

1. Introduction

Semiconductor injection lasers emitting at 0.8 μm are promising radiation sources for open communication systems and pumping solid-state and fibre lasers. It is well known that the basic energy characteristics of modern laser diodes such as the output power, efficiency, and slope efficiency can be close to the limiting values. Nevertheless, a number of the laser parameters are still far from perfect and are the subject of investigations. Among them is the optical beam quality, which is most simply characterised by the beam divergence. It is obvious that the minimum divergence of any optical beam is physically determined by diffraction from its aperture (beam diameter). However, the real divergence of the beam from a high-power laser diode is usually a few or even tens times exceeds the diffraction-limited divergence. The high-quality 200-mW, 0.98-μm laser beam with the nearly diffraction-limited divergence was obtained in [1] due to optimisation of the ridge waveguide of the laser resonator.

In this paper, we use the approach developed in [1] for the development of a high-power single-mode laser emitting at 0.8 μm. Because the operating regime of the laser is sensitive to the waveguide parameters, which in turn depend on the characteristics of a particular multilayer heterostructure, the additional studies were required, which are presented below. In addition, the question about the accuracy of representing the real two-dimensional intensity distribution of ridge lasers in the factorised form, i.e., as a product of two one-dimensional distributions for mutually perpendicular transverse distributions has remained unclear in [1]. This problem was also studied in our paper.

S.A. Plisyuk, I.V. Akimova, A.E. Drakin, A.P. Bogatov P.N. Lebedev Physics Institute, Russian Academy of Sciences, Leninskii prosp. 53, 119991 Moscow, Russia; e-mail: bogatov@sci.lebedev.ru;
A.V. Borodaenko, A.A. Stratonnikov Moscow Institute of Physics and Technology (State University), Institutskii per. 9, 141700 Dolgoprudnyi, Moscow region, Russia;
V.V. Popovichev M.F. Stel'makh Polyus Research & Development Institute, ul. Vvedenskogo 3, 117342 Moscow, Russia

Received 5 April 2005
Kvantovaya Elektronika **35** (6) 515 – 519 (2005)
Translated by M.N. Sapozhnikov

2. Experimental

Parameters of the layers of a heterostructure containing a quantum-well active layer, which was used in the lasers under study, are presented in Table 1. The waveguide effect in the horizontal plane was provided by a ridge in the form of a trapeze with the widths of the top and bottom bases equal to 3.5 and 5 μm, respectively. The residual etching width (outside the ridge) of the p-emitter layer found during optimisation by the method developed in [1] was 0.4 μm for the structure parameters presented in Table 1. The lasers under study had the resonator length of 1 mm and the reflectivities of the highly reflecting and output mirrors equal to 97 % and 2 %, respectively. The laser wavelength was approximately 812 nm. All the measurements were performed at room temperature in the cw lasing regime.

The far-field intensity distribution of the laser was recorded by using an automated setup [2]. The light – current characteristic was measured with a thermocouple with a set of filters. Spectral measurements were performed with a DFS-12 monochromator equipped with a CCD linear array mounted at the monochromator exit slit. The data accumulation time was $\sim$0.5 s. The accuracy of measuring the spectral component wavelength was limited by the array pixel size, $\sim$4 pixels corresponding to one lasing mode.

The field distribution on the output mirror of the laser was recorded with an optical system shown in Fig. 1. The image of the output end-face of the diode was focused on the CCD array of a video camera by a 235$^\times$ planachromate $0/\infty$ microobjective with the numerical aperture 0.65. The output signal of the video camera was detected with a video board in a computer. The light flux was attenuated with the help of mirror attenuators representing the faces of glass prisms without special coatings. This provided the required attenuation of the optical beam by preserving its quality and signal linearity at the flux densities on the output mirror of the laser exceeding 10^7 W cm^{-2}.

The results of near-field intensity measurements were recorded in the form of a raster image in the computer. Then, the 2D constant-intensity levels were constructed.

Table 1.

Layer	Composition	Layer thickness/μm	Refractive index	Dopant concentration/cm^{-3}
Contact	GaAs : Zn	0.4	3.659	2×10^{19}
Cladding	p-$Al_{0.37}Ga_{0.63}As$: Zn	1.8	3.384	7.4×10^{17}
Waveguide	$Al_{0.31}Ga_{0.69}As$	0.12	3.427	–
Active	$Al_{0.08}Ga_{0.92}As$	0.011	3.657	–
Waveguide	$Al_{0.31}Ga_{0.69}As$	0.12	3.427	–
Cladding	n-$Al_{0.37}Ga_{0.63}As$: Si	2.4	3.384	7×10^{17}
Buffer	GaAs : Si	0.5	3.659	1.5×10^{18}
Substrate	n-GaAs : Si	100	3.659	2×10^{18}

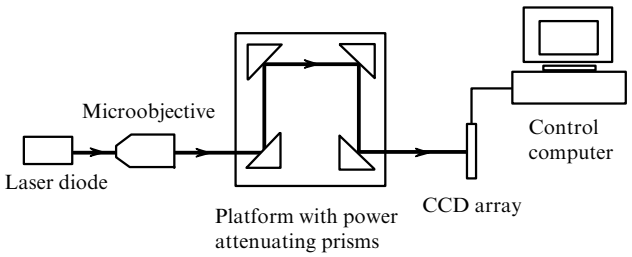

Figure 1. Scheme of the optical setup for near-field measurements.

(The two-dimensional near-field intensity pattern gives a more detailed description of the laser field in the resonator than the method of integrated averaging along one of the directions.) The near- and far-field intensity distributions obtained in experiments were used to calculate the M^2 factor by the method described in [1]. The value of the M^2 factor characterises the optical beam quality.

3. Experimental results and discussion

Figure 2 shows the typical far-field intensity distributions $\Phi(\phi)$ in the vertical plane for two pump currents. One can see that $\Phi(\phi)$ is almost independent of the pump current. This suggests that a change in the permittivity ε in the active layer depending on the concentration of injected carriers and a thermal change in ε are considerably lower that the permittivity jump at the boundaries of heterostructure layers. Figure 2 also presents the far-field intensity distribution in the vertical plane calculated for a planar waveguide with the layer parameters given in Table 1. The calculated distribution proves to be somewhat narrower than the experimental distributions. The experimental and calculated distributions can be made coincident by varying the refractive indices of the waveguide layers of the structure within the technological error ($\sim$2 %) of measuring the layer composition. This means that a slight discrepancy between the calculated and experimental vertical intensity distributions has a technological nature.

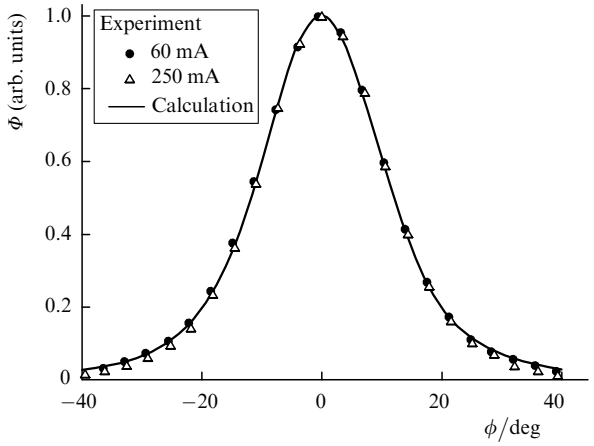

Figure 2. Far-field laser radiation intensity distributions $\Phi(\phi)$ in the vertical plane for different pump currents.

The experimental and calculated far-field intensity distributions $I(\psi)$ for the horizontal plane (along the p–n junction) are presented in Fig. 3. The intensity distribution $I(\psi)$ was calculated in the 'effective' refractive index approximation by the method described in [1]. The geometrical parameters of the ridge profile were obtained by processing the photographs of the output mirror of the laser obtained with the help of a scanning electron microscope.

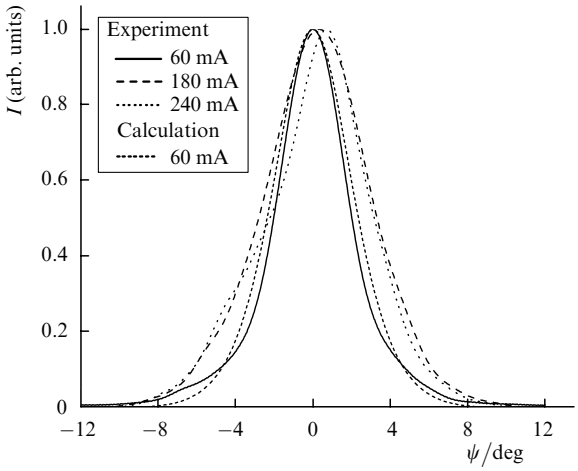

Figure 3. Far-field laser radiation intensity distributions $I(\psi)$ in the horizontal plane for different pump currents.

The corresponding near-field intensity distributions are shown in Fig. 4. In the case of the horizontal intensity distribution, good agreement between calculations and experiment is observed. The discrepancy observed for the vertical distribution is explained by the fact that the calculated near-field distribution in this direction is narrower than the instrumental function of the microobjective (Fig. 4a). The experimental near-field intensity distribution in the vertical direction is in fact a convolution of the real distribution with the instrumental function of the objective. Because the experimental and calculated radiation patterns in this plane are in good agreement (Fig. 2), we can assume

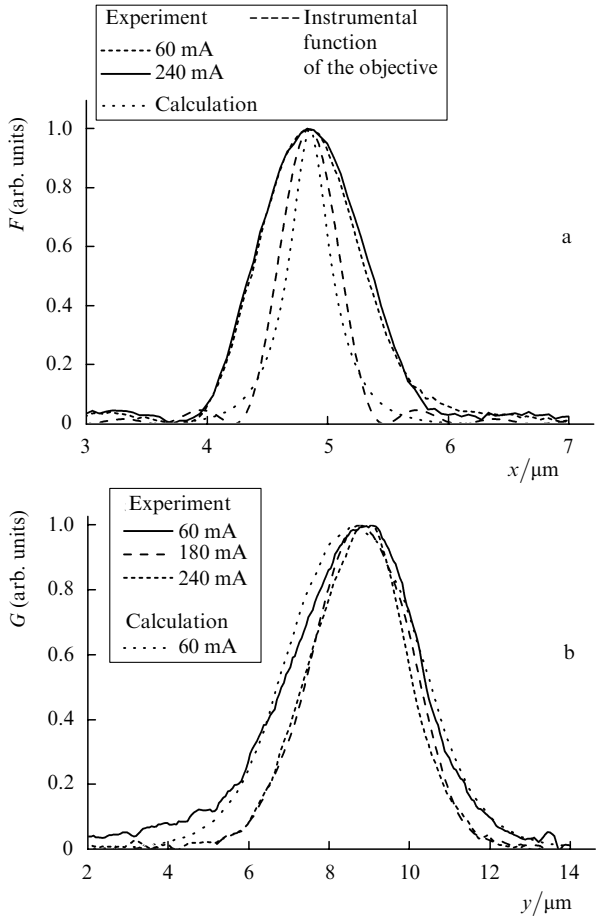

Figure 4. Near-field laser radiation intensity distributions in the vertical $F(x)$ (a) and horizontal $G(y)$ (b) planes for different pump currents.

that the real near-field intensity distribution in the vertical direction is also close to the calculated distribution.

Figure 3 shows that the experimental far-field intensity distribution obtained for the pump current close to the threshold (60 mA) virtually coincides with the calculated distribution. The discrepancy at the 10 % level can be explained by inaccuracies in the consideration of the current flow and determination of the temperature profile in the laser diode. As the pump current was increased up to $\sim$180 mA, the distribution curve broadened, preserving its bell-shaped profile. This means that the near-field intensity distribution narrows down. As mentioned earlier [1], this behaviour is explained by the increase in the waveguide effect in the horizontal plane caused by the spatial burning of carriers and heating of the waveguide layers. Indeed, due to the spatial burning of carriers caused by stimulated transitions, their concentration near the resonator axis is drastically reduced with increasing optical power and tends to the concentration at which the bleaching of the layer occurs. At the same time, the concentration in peripheral regions (at the mode 'wings') will, on the contrary, increase with increasing optical power. This is explained by the fact that the concentration should retain its threshold value on the average. Finally, the refractive index profile induced by carriers is formed, which causes the increase in the horizontal waveguide effect. In addition, because of a more intense heating of the active region at the beam centre compared to the adjacent passive regions, an additional optical waveguide is also formed, which is already induced by the spatial temperature profile and is characterised quantitatively by the positive coefficient $\partial n/\partial T$ of the temperature dependence of the refractive index. These two processes cause the above 'compression' of the optical beam in the horizontal direction.

For the pump current above 180 mA, the change in the waveguide properties of the resonator is so strong that the far-field intensity distribution becomes asymmetric. It seems that upon a strong inversion burning, the horizontal distribution of the optical flux becomes very sensitive to random defects of the waveguide, for example, to the ridge asymmetry due to self-action. Nevertheless, we see that the field distribution remains transversely single-mode, as follows from the spectrum in Fig. 5, which corresponds to the single-frequency lasing. Note here that the 'compression' of the optical beam is also accompanied by the passage from multimode to single-mode lasing (Fig. 5).

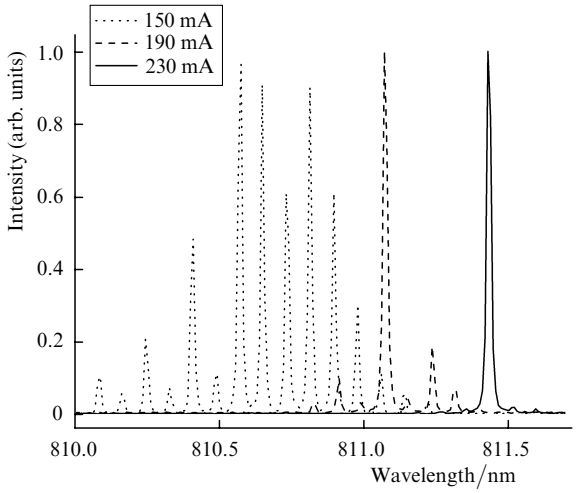

Figure 5. Emission spectra of the laser for different pump currents.

Such a spectral behaviour can be explained by the fact that the transverse homogeneity of the irradiated active medium improves upon beam compression. Indeed, if the optical beam diameter is comparable with the diffusion length of carriers, we can assume that the concentration of carriers over the beam section is almost constant. As a rule, the improvement of the spatial homogeneity favours singe-frequency lasing. Another factor responsible for such behaviour can be the passage from the regime of undamped intensity pulsations, which is typical for a laser with a 'weak' waveguide, to stationary lasing upon the enhancement of the waveguide properties of the resonator. It is well known that in the pulsation regime lasing occurs at many longitudinal modes [3, 4], whereas stationary lasing with a stable transverse field distribution has also a higher stability of the single-frequency lasing regime upon increasing the output power [5].

Figure 6 shows the constant normalised intensity lines characterising the two-dimensional near-field intensity distribution. Figure 7 demonstrates the two-dimensional factorised distribution calculated from the experimental one-dimensional distributions $F(x)$ and $G(y)$ by the expression

$$I(x, y) = F(x)G(y).$$

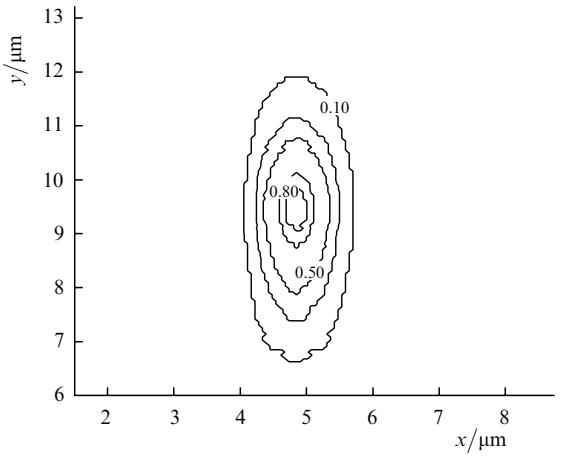

Figure 6. Experimental two-dimensional near-field normalised laser intensity distribution.

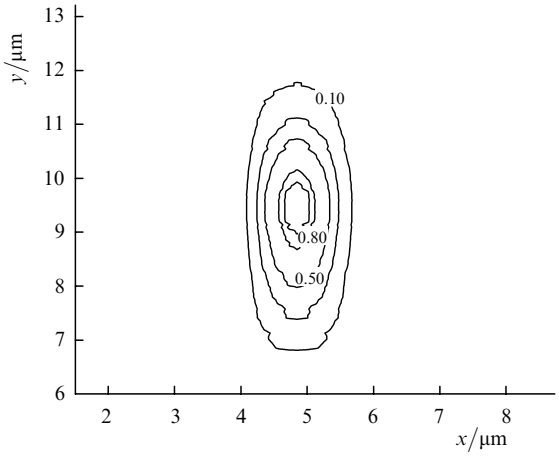

Figure 7. Factorised two-dimensional near-field normalised intensity distribution obtained by multiplying two one-dimensional distributions $F(x)$ and $G(y)$.

A comparison of distributions in Figs 6 and 7 shows that the factorised 2D distribution well corresponds to the real near-field intensity 2D distribution. These distributions for the ridge laser coincide within the measurement error.

Figure 8 shows the typical light–current characteristic for these lasers with the indicated values of the M^2 factor. This characteristic is linear within the measurement error and $M^2 \approx 1.1$. It is accepted that for $M^2 \leqslant 1.1$ the beam has the diffraction-limited divergence.

An important characteristic of each laser is its reliability. We determined the service life of the lasers at three different temperatures and the constant pump current providing the initial output power of 150 mW. Typical results of such tests are presented in Fig. 9. The output power decreased by no more than 3 % after 1000 h, which is quite acceptable for many practical applications.

4. Conclusions

The optimisation of the ridge waveguide in the 0.98-μm heterolaser [1] and the 0.81-μm heterolaser manufactured in this work provided single-mode lasing with the output power up to 200 mW by preserving the diffraction-limited

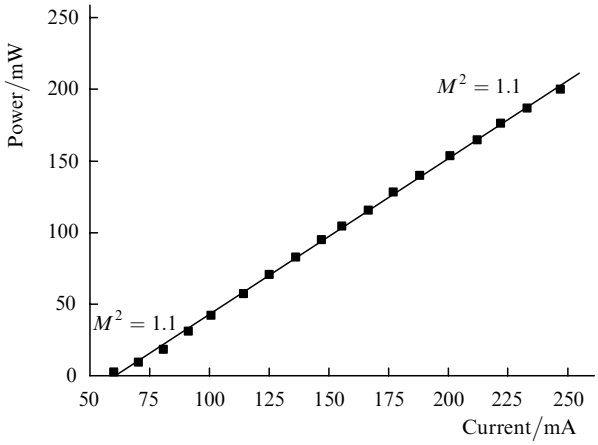

Figure 8. Typical light–current characteristic of a 0.812-μm high-brightness laser. The value $M^2 = 1.1$ is invariable over the entire radiation power range.

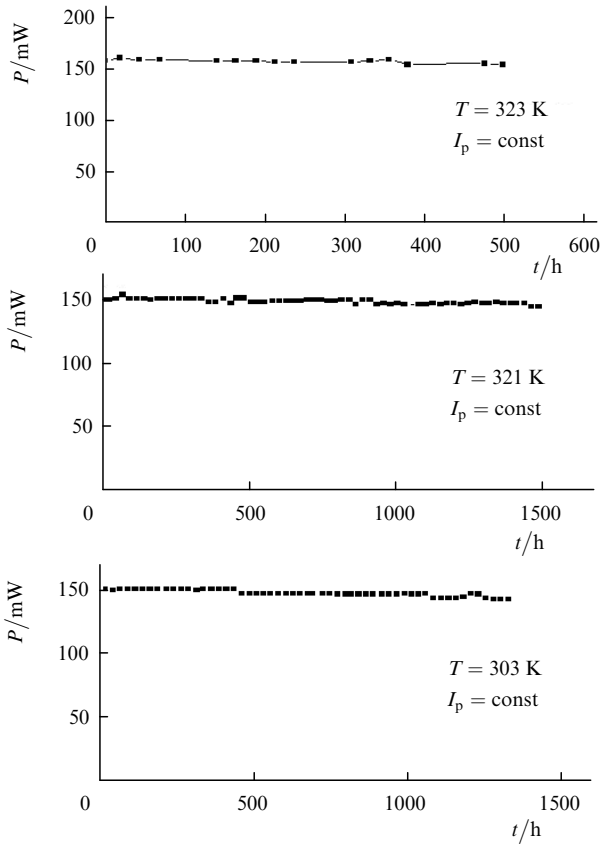

Figure 9. Dependences of the output power of the laser on the operation time at a constant pump current at three temperatures.

divergence of the laser beam. In each of these lasers, different heterostructures were used and the optimal geometries of the ridges were different. A common feature is that the optimisation can be performed for each structure within the framework of the same approach, by using the effective refractive index method. Note that although the beam quality of the lasers corresponds to the diffraction limit, nevertheless the parameters of this beam somewhat vary at high powers ($\sim$180 mW). This circumstance is undesirable for a number of applications and is the subject of a further improvement of the laser design.

We have shown that the two-dimensional near-field intensity distribution for the lasers studied in the work can be represented with a good accuracy in the factorised form as a product of the two corresponding one-dimensional distributions. This can considerably simplify both the simulation of the intensity distribution over the beam section and the detection of the 2D intensity distribution for ridge lasers.

Our experiments have shown that an increase in the power in the single-mode lasing regime leads to the establishment of single-frequency lasing, i.e., to the regime in which all the axial modes, except the laser mode, are suppressed.

Acknowledgements. This work was partially supported by the Presidium of the Russian Academy of Sciences within the framework of programs 'Low-dimensional quantum structures' and 'Semiconductor lasers'.

References

1. Popovichev V.V., Davydova E.I., Marmalyuk A.A., Simakov A.V., Uspenskii M.B., Chel'nyi A.A., Bogatov A.P., Drakin A.E., Plisyuk S.A., Stratonnikov A.A. *Kvantovaya Elektron.*, **32**, 1099 (2002) [*Quantum Electron.*, **32**, 1099 (2002)].
2. Bogatov A.P., Drakin A.E., Stratonnikov A.A., Konyaev V.P. *Kvantovaya Elektron.*, **30**, 401 (2000) [*Quantum Electron.*, **30**, 401 (2000)].
3. Bogatov A.P., Eliseev P.G., Panteleev V.I., Shevchenko E.G. *Kvantovaya Elektron.*, No. 5, 93 (1971) [*Sov. J. Quantum Electron.*, **1** (5), 500 (1971)].
4. Bogatov A.P., Eliseev P.G., Manko M.A., Ivanov L.P., Logginov A.S., Senatorov K.Ya. *IEEE J. Quantum Electron.*, **9** (2), 392 (1973).
5. Batrak D.V., Bogatov A.P., Kamenets F.F. *Kvantovaya Elektron.*, **33**, 941 (2003) [*Quantum Electron.*, **33**, 941 (2003)].